

ScienceDirect



IFAC PapersOnLine 58-28 (2024) 636-641

A Study on Control Co-Design for Optimizing Microgrid Sustainability

Tania Rifat Jahan*, Asmaou S. Ouedraogo*, Donald J. Docimo*

*Mechanical Engineering Department, Texas Tech University, Lubbock, TX 79407 USA (e-mail: tjahan@ttu.edu, aouedrao@ttu.edu, donald.docimo@ttu.edu)

Abstract: This paper studies the optimization of microgrid plant and controller features to reduce environmental impacts. The configuration and control of grid technology is critical for storing and supplying energy. While these systems are traditionally designed for maximizing efficiency and frequency regulation, there is a shift towards minimizing grid environmental footprints. This work presents a framework to enable sustainability-centric microgrid design, with two main features. The first is the inclusion of control co-design (CCD), which expands the design space and potential capabilities of the microgrid. The second is the introduction of sustainability-centric objective functions, categorized into environmental impact from microgrid component manufacturing, operation, and disposal. After introducing the candidate microgrid's model, controller, and CCD framework, the system is optimized to support a data center during a blackout. The relationship between the sustainability objective functions and the plant and controller design variables are explored. Pareto fronts are identified and studied, providing a comparison of the influence of each sustainability category on environmental impact.

Copyright © 2024 The Authors. This is an open access article under the CC BY-NC-ND license (https://creativecommons.org/licenses/by-nc-nd/4.0/)

Keywords: Microgrid, Control Co-Design, Sustainability, Data Center

1. INTRODUCTION

This paper explores the connection between plant features, controller parameters, and sustainability for optimization of microgrid systems. Microgrid-based technology is expected to propel the next generation of the energy sector, facilitating integration of heterogeneous energy producing components and stand-alone power delivery. However, while grid-side supply and storage continue to evolve, so too do power demands. Consider data centers, which consume 1-2% of global energy produced (Shehabi *et al.*, 2016; Fuchs *et al.*, 2020), with that percentage expected to increase over the next decade (Koot and Wijnhoven, 2021). Such large-scale power loads for microgrid systems raise concerns not only with energy efficiency, but also environmental impact and sustainability. This reformulates the requirements when designing, building, and managing grid systems.

There are multiple pathways for yielding microgrid designs that meet the increasing standards and expectations. We break these pathways up into two broad categories:

(1) Design space expansion: System outcomes are often enhanced by expanding the design variables considered. This includes consideration of nontraditional plant features, such as photovoltaic (PV) farm and battery bank size, within optimal sizing procedures (Alramlawi and Li, 2020; Masaud and El-Saadany, 2020). This also includes alterations to microgrid supervisory management, with examples including optimal PI controller design (Abou El-Ela, Mosalam and Amer, 2023) and model predictive control (Parisio and Glielmo, 2011). A small number of studies simultaneously optimize plant and controller parameters, known as control co-design (CCD). CCD can support new system capabilities, such as hybrid tidal-solar-battery integration (Cohen et al., 2023).

(2) Objective function diversification: The changes in expectations of microgrid capabilities can be captured by changes to the objectives. Traditional objectives for a microgrid controller include stabilization and frequency regulation (Wang et al., 2020; Aazami et al., 2022), as well as matching power supply and demand (Zhao and Ding, 2018). Plant sizing objective functions often reflect cost, such as through a levelized cost of energy (Pandit et al., 2021). A greater emphasis has been placed on inclusion of greenhouse gas (GHG) emissions (Barakat, Ibrahim and Elbaset, 2020; Attia et al., 2021), which is often combined with energy, capital, and maintenance expenses (Yan et al., 2017).

While progress has been made to adapt microgrid designs for the future of the energy sector, several gaps have been left unaddressed. First, microgrid CCD remains limited in scope. Second, sustainability-related metrics are often regulated to a small piece of the optimization problem, rather than a focus. In comparison to previous studies, this paper presents sustainability-centric CCD for microgrid optimization. Through this, CCD methods are broadened to support microgrid plant and controller parameter optimization, expanding the microgrid design space. Within the CCD framework, objective functions are defined to quantify and emphasize sustainability at three life stages of microgrid components: manufacturing, operation, and disposal. This framework is set to facilitate superior microgrid design and control, reflecting the requirements of the future energy sector.

To develop the sustainability-centric CCD framework, an outline of the baseline microgrid model and controller is presented (Section 2). Next, the CCD optimization problem is formulated (Section 3). Within this, sustainability objective functions are defined as relating to the three identified microgrid component lifecycle stages. A test case of optimizing the microgrid to power a data center during a

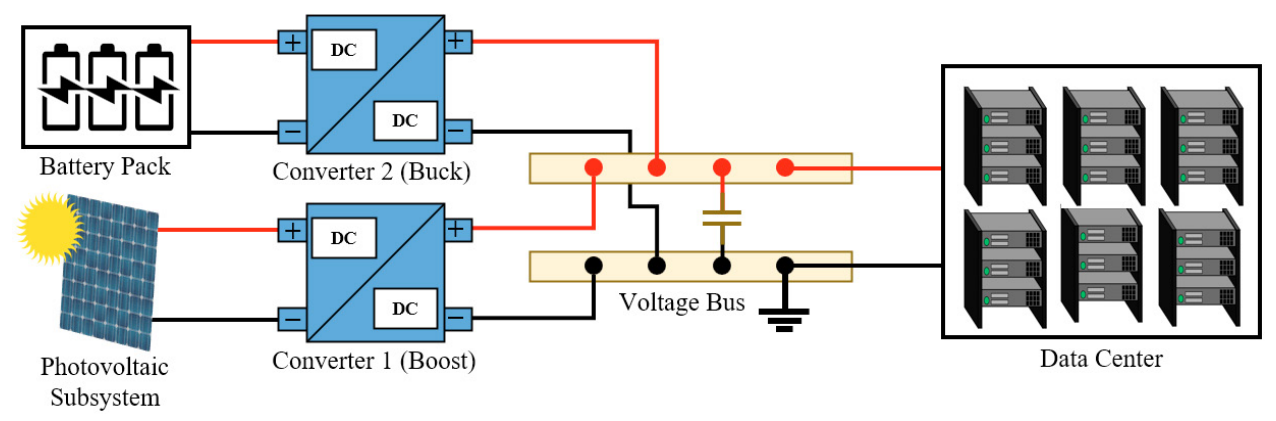


Figure 1. Microgrid plant configuration.

blackout is explored, with relationships between the design variables and objective functions determined (Section 4). Finally, the paper ends with a summary of the major elements presented and future steps (Section 5).

2. MICROGRID DYNAMICS AND CONTROLLER

This section summarizes the baseline configuration of the microgrid and the control algorithm that manages the system dynamics. The microgrid model consists of five components, each described by a set of differential algebraic equations (DAEs). The baseline control algorithm developed is built to track desired state and power demand references using a model-free approach.

2.1 Microgrid Plant Model

Figure 1 presents the configuration of the candidate microgrid. For this study, the primary purpose of the microgrid is to meet the data center power demand during a 24-hour blackout scenario. Components are modeled as DC elements, with the methods applicable to AC components. The first component is the voltage bus, which acts as a bridge connecting all power supply and demand flows. The bus, with voltage state V_{bus} , consists of a capacitor with capacitance $C_{bus} = 1000$ F. The state equation, based on the conservation of energy, is:

$$\dot{V}_{bus} = \frac{1}{c_{bus}} \left(I_{out,1} + I_{out,2} - u_0 I_{load} - \frac{V_{bus}}{R_{b,1}} \right). \tag{1}$$

The first two terms on the right side of (1) are the output currents of the two converters, $I_{out,i}$ for $i \in [1..2]$, defined as:

$$I_{out,i} = \frac{1}{R_{h,2}} \left(V_{out,i} - V_{bus} \right), \tag{2}$$

with converter output voltage state $V_{out,i}$, and resistance $R_{b,2} = 10^{-4}\Omega$ used to capture inefficiencies. Note that the differences between the output and bus voltages are very small. The third term in (1) contains I_{load} , the load current from the data center, and u_0 , a duty cycle control input that throttles power to the data center. The power to the data center is defined as $P_{load} = u_0 I_{load} V_{bus}$. Figure 2 presents a power demand profile $P_{load,ref}$ for a data center (Wang *et al.*, 2012), scaled to have a peak power of 1 MW. The final term of (1) captures additional power dissipation from the bus, with resistance $R_{b,1} = 10^4 \Omega$.

Each DC-DC converter has an input current $I_{in,i}$, input voltage $V_{in,i}$, output current $I_{out,i}$, output voltage $V_{out,i}$, and duty cycle

 u_i . The duty cycles act as the control inputs for regulating the voltages. Capacitors, with C=1000 F, are placed in parallel with each input and output connection, and resistors $R_{c,1}=10^4\Omega$, $R_{c,2,1}=5\times10^{-5}\Omega$, and $R_{c,2,2}=5\times10^{-4}\Omega$ capture converter inefficiencies. The boost converter (i=1) connects the PV subsystem to the bus, stepping up $V_{out,1}$ from $V_{in,1}$:

$$\dot{V}_{in,1} = \frac{1}{c} \left(I_{in,1} - \frac{V_{in,1}}{R_{c,1}} - \frac{1}{R_{c,2,1}} (V_{in,1} - u_1 V_{out,1}) \right),
\dot{V}_{out,1} = \frac{1}{c} \left(\frac{u_1}{R_{c,2,1}} (V_{in,1} - u_1 V_{out,1}) - \frac{V_{out,1}}{R_{c,1}} - I_{out,1} \right).$$
(3)

The buck converter (i = 2) connects the Li-ion battery pack to the bus. This converter drops the voltage from input to output:

$$\dot{V}_{in,2} = \frac{1}{c} \left(I_{in,2} - \frac{V_{in,2}}{R_{c,1}} - \frac{u_2}{R_{c,2,2}} \left(u_2 V_{in,2} - V_{out,2} \right) \right),
\dot{V}_{out,2} = \frac{1}{c} \left(\frac{1}{R_{c,2,2}} \left(u_2 V_{in,2} - V_{out,2} \right) - \frac{V_{out,2}}{R_{c,1}} - I_{out,2} \right).$$
(4)

The PV subsystem consists of 20000 solar panels in parallel. Equations (5) presents the thermal dynamics for a single PV module (Jones and Underwood, 2001; Docimo, Ghanaatpishe and Mamun, 2017). The parameters C_m =4580 J/K, $\alpha_{PV}=0.7$, $A_S=0.8~{\rm m}^2$ and $h=13.4~{\rm w\over m^2 K}$ are the lumped thermal capacitance, absorptivity, module surface area, and convection coefficient, respectively. This equation shows how PV temperature T_{PV} is impacted by irradiation G, ambient temperature T_{∞} , and output electrical power $P_{PV}=I_{PV}V_{PV}$. Note that $I_{in,1}=I_{PV}$ and $V_{in,1}=V_{PV}$. The current I_{PV} is dependent on T_{PV} , G, and V_{PV} , with the nonlinearity and parameters defined in (Villalva, Gazoli and Filho, 2009):

$$\dot{T}_{PV} = \frac{1}{c_m} (\alpha_{PV} A_s G - h A_s (T_{PV} - T_{\infty}) - I_{PV} V_{PV}). \quad (5)$$

The Li-ion battery pack is composed of $N_{ser,Li} = 112$ and $N_{par,Li}$ lithium iron phosphate cells in series and parallel, respectively. An equivalent circuit model is used to describe the battery dynamics, with the states including the state of charge (SOC) and relaxation voltages $V_{p,Li}$ for p = [2,3,4]. The Li-ion battery cell's dynamics, with battery current $I_{Li} = I_{in,2}$ and battery cell voltage $V_{Li} = V_{in,2}$ can be summarized in:

$$S\dot{O}C = -\frac{I_{Li}}{Q_{Li}},\tag{6}$$

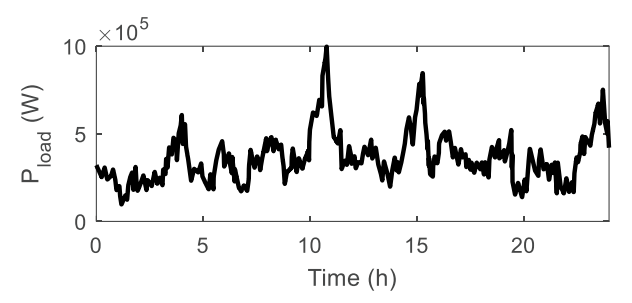


Figure 2. Scaled data center power demand (Wang et al., 2012).

$$\dot{V}_{p,Li} = \frac{1}{C_{p,Li}} \left(I_{Li} - \frac{V_{p,Li}}{R_{p,Li}} \right),$$
 (7)

$$V_{Li} = OCV_{Li}(SOC) - V_{2,Li} - V_{3,Li} - V_{4,Li} - I_{Li}R_{1,Li}.$$
 (8)

The nominal capacity for a cell is $Q_{Li} = 1.21$ Ah. The capacitances are $C_{2,Li} = 15000$ F, $C_{3,Li} = 8000$ F, and $C_{4,Li} = 550$ F, and the resistances are $R_{1,Li} = 0.0192$ Ω , $R_{2,Li} = 0.219$ Ω , $R_{3,Li} = 0.0257$ Ω , and $R_{4,Li} = 0.0331$ Ω . Figure 3 presents the open-circuit voltage, OCV_{Li} , as a function of SOC.

Combining these component models creates the microgrid representation as a set of DAEs. As noted in previous work, it is possible to convert these dynamics into a conservation of energy-based graphical model, with storage capacitance matrix C, incidence matrix \overline{M} , and nonlinear power flows P (Pangborn *et al.*, 2018; Laird *et al.*, 2022):

$$C\dot{x} = -\overline{M}P(x, u, x^s). \tag{9}$$

The 15 \times 1 state vector \boldsymbol{x} consists of the states, such as V_{bus} , T_{PV} , and SOC. The 3 \times 1 control input vector \boldsymbol{u} contains the duty cycles u_0 , u_1 , and u_2 . The 7 \times 1 external state vector \boldsymbol{x}^s consists of exogeneous inputs and disturbances, such as I_{load} and T_{∞} . This compact representation supports the CCD framework of Section 3.

2.2 Control Algorithm

The purpose of the control algorithm is to determine the next set of duty cycle values after each timestep Δt . This work utilizes a model-free procedure based on perturb and observe methods (Ali *et al.*, 2020). Figure 4 presents the generalized procedure. At each timestep, a duty cycle u_j , with integer $j \in [0..2]$, is perturbed by an amount $-\Delta u$, 0, or $+\Delta u$, with Δu as a constant. After observing the change in the system from the previous to the current timestep, quantified by α and β , the input is perturbed again to track the desired outcome for α . This process repeats continuously, keeping the inputs within their limits. There are three control modes:

(a) In the nominal mode, the input associated with the data center, u_0 , is adjusted to track the power demand. To implement this with j=0 and time index k, the terms in the flowchart of Figure 4 become $\alpha_0 = P_{load,ref,k} - P_{load,k}$ and $\beta_0 = u_{0,k} - u_{0,k-1}$. In addition, PV output power is maximized in the nominal mode, with $\alpha_1 = P_{PV,k} - P_{PV,k-1}$ and $\beta_1 = V_{PV,k} - V_{PV,k-1}$ to determine u_1 . The buck converter input u_2 is set to a constant.

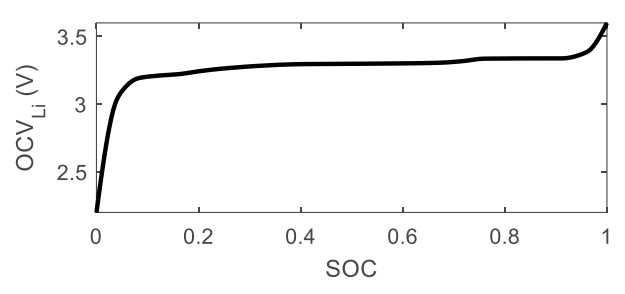


Figure 3. Open-circuit voltage of the Li-ion battery.

- (b) If $SOC > SOC_{max}$, then the PV is shut off to avoid overcharging the battery, with $u_1 = 0$. To return to a safe operating mode for the battery, the buck converter is used to track a desired SOC_{ref} . With this, $\alpha_2 = SOC_{ref,k} SOC_k$ and $\beta_2 = u_{2,k} u_{2,k-1}$.
- (c) Similarly, if $SOC < SOC_{min}$, data center power tracking is turned off to avoid undercharging the battery, so $u_0 = 0$. Again, SOC tracking is implemented.

3. SUSTAINABILITY-CENTRIC CONTROL CO-DESIGN

This section presents the CCD framework used for sustainability-centric optimization of microgrids. First, the plant and controller design variables are defined. Second, the objective functions are presented, divided into three categories related to sustainability. Third, the constraints of the optimization problem are summarized.

3.1 Design Variables

To expand the design space for microgrid optimization, the framework of this paper explicitly includes both plant and controller parameters. Plant design variables, $\boldsymbol{\theta}$, include both sizing- and topology-related parameters. Appropriate microgrid examples include the number of PVs, types and configurations of the battery packs, and converter dimensions. Controller design variables, $\boldsymbol{\phi}$, can include the control architecture, timestep, horizon for predictive algorithms, weights, and gains. For this work, one of each type of design variable is considered, supporting analysis of identified designs without loss of generality. The plant design variable is the number of Li-ion cells in parallel, $\boldsymbol{\theta} = \boldsymbol{\theta} = N_{par,Li}$. The controller design variable is the duty cycle perturbation magnitude, $\boldsymbol{\phi} = \boldsymbol{\phi} = \Delta u$.

3.2 Objective Functions

One of the most critical metrics for future microgrids is the ability of the system to support environmental sustainability. Expanding beyond the typical viewpoint presented in the microgrid literature, we define three essential categories of sustainability objective functions: manufacturing, operations, and disposal. The manufacturing objective, J_m , relates to direct and indirect environmental impacts from building and assembling microgrid components. Depending on the component and energy source used for manufacturing, this can generate the highest GHG emissions from all lifecycle stages of the microgrid component (Larcher and Tarascon, 2015). For this work, the function is defined as:

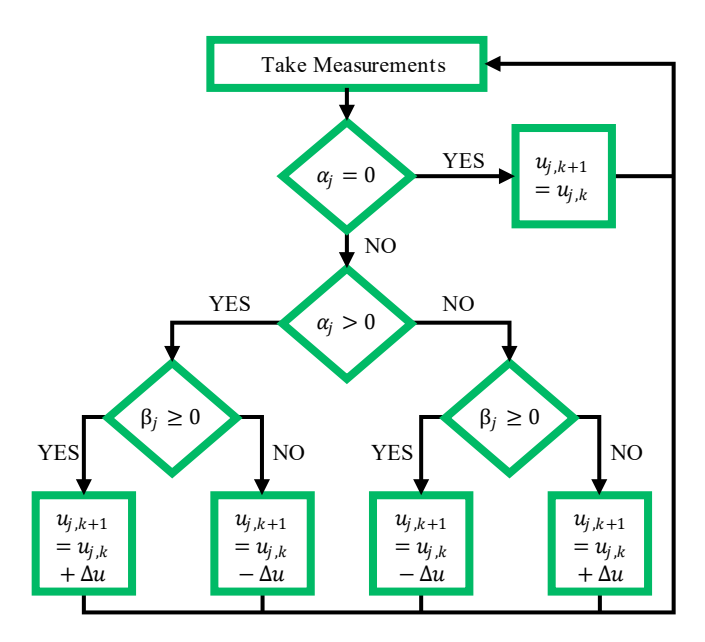


Figure 4. Logic of the perturb & observe control algorithm.

$$J_m = c_m \theta, \tag{10}$$

where $c_m = 224 \, \mathrm{kgCO}_{2,\mathrm{e}}/\mathrm{cell}$ is determined using values from (Hao *et al.*, 2017) to convert the size of the battery pack into equivalent CO₂ (CO_{2,e}) released. The operations objective, J_o , quantifies environmental impacts due to operation of the microgrid. For the system and blackout scenario considered in this work, no fossil fuels are used. Total wasted energy into the environment is considered the impact from operations:

$$J_o = c_o \int_0^{t_f} P_{out}(\tau) d\tau. \tag{11}$$

In (11), P_{out} is the sum of all waste heat terms from (9), and t_f is the final time. The coefficient $c_o = 3.7 \times 10^{-9} \, \mathrm{kgCO_{2,e}}/\mathrm{J}$ converts the wasted energy into kg of $\mathrm{CO_{2,e}}$, using the knowledge that waste heat has a fraction of an impact as $\mathrm{CO_{2}}$ release does over a century (Zevenhoven and Beyene, 2011). The disposal objective, J_d , quantifies impact from disposing of microgrid components at the end-of-life. This can relate to recycling and electronic waste (e-waste). For this work, higher battery degradation is used to represent earlier component failure, replacement, and disposal. The capacity loss of a cell, Q_{loss} , is dependent on the battery SOC and current, with this nonlinear dynamic described in (Ramadass *et al.*, 2004; Docimo and Fathy, 2017):

$$J_d = Q_{loss}(SOC, I_{Li}). (12)$$

The individual objective functions can be combined into a total objective, J_{tot} , with weights w_m , w_o , and w_d . With n > 1 used for compromise programming, J_{tot} can be expressed as:

$$J_{tot} = w_m J_m^n + w_o J_o^n + w_d J_d^n.$$
 (13)

3.3 Constraints

The first constraint for the CCD problem ensures the scaled microgrid model dynamics are obeyed. Inclusion of the plant design variables is equivalent to augmenting the graph-based model of (9):

$$\Psi_c(\theta)C\dot{x} = -\overline{M}\Psi(\theta)P(x, u, x^s), \tag{14}$$

where $\Psi_c(\theta)$ and $\Psi(\theta)$ are diagonal matrices that scale the parameters of the plant (Docimo *et al.*, 2021). The second constraint relates to the controller, which depends on the controller design variables. A compact representation of the controller presented in Section 2.2 is:

$$u_{k+1} = f(\phi, u_k, u_{k-1}, x_k, x_{k-1}, P_k, P_{k-1}, x_{ref,k}, P_{ref,k}), (15)$$

with x_{ref} and P_{ref} as the reference state and power flow vectors. With the emphasis on sustainability within the objective function, power tracking for the data center is related to the constraints. The third constraint defines a maximum total tracking error, $\bar{\mu}_{tr}$, differentiating acceptable and unacceptable designs:

$$\int_0^{t_f} \left(P_{load,ref}(\tau) - P_{load}(\tau) \right)^2 d\tau \le \bar{\mu}_{tr}. \tag{16}$$

The final constraints bound the design variables to minimum $(\theta_{min}, \phi_{min})$ and maximum values $(\theta_{max}, \phi_{max})$:

$$\theta_{min} \le \theta \le \theta_{max},
\phi_{min} \le \phi \le \phi_{max}.$$
(17)

Given initial conditions for the states, the CCD optimization problem is defined to determine the θ and ϕ values that minimize (13). This is subject to the numerical solutions of (14)-(16) and (17).

4. RESULTS

This section presents the results from applying the CCD framework to the defined microgrid. To confirm the controller is able to perform properly, the system is tested with preliminary values for the design variables. Solutions to the CCD problem are then determined through a grid search of the design space. The relationship between the design variables and sustainability objectives, as well as Pareto solutions, are explored.

4.1 Controller Validation

To confirm the controller is able to track the data center power demand (Figure 2) and limit SOC bound violations, the microgrid model and control algorithm are evaluated with baseline parameters. The design variables are set to θ as 10000, 12000, and 14000, and ϕ as 0.01. The remaining controller parameters are defined as $\Delta t = 60$ s, $SOC_{min} = 0.1$, $SOC_{max} = 0.9$, and $SOC_{ref} = 0.5$. A sinusoidal irradiation profile is used with $T_{\infty} = 25$ °C. While $t_f = 24$ hr is used, results approximately reflect long-term sustainability criteria. The MATLAB function ode23tb is used for simulation.

Figure 5 presents P_{load} , SOC, and the energy produced from the PV, E_{PV} , over time. This figure provides two pieces of information. The first piece is that the controller behaves as expected. The data center power demand is tracked within acceptable tolerances, with all three designs having nearly identical outputs through the first 20 hours. When SOC reaches SOC_{max} , energy from the PV is reduced. For some of the designs, SOC hits SOC_{min} , shutting off power to the data center. This leads to the second piece – smaller battery pack

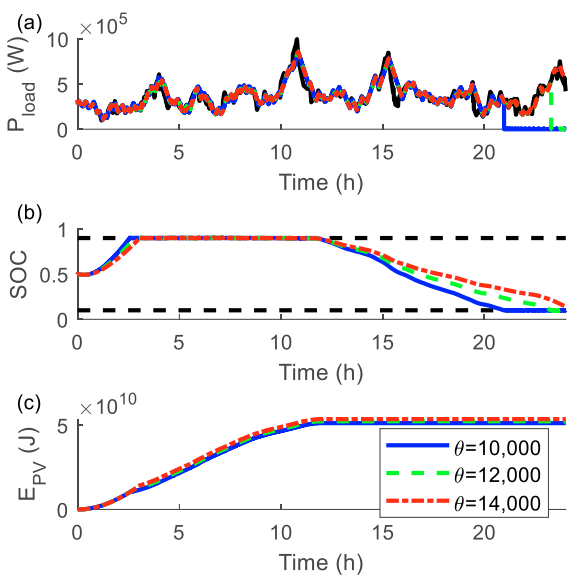


Figure 5. Microgrid (a) data center power, (b) battery SOC, and (c) energy out of the PV with $\phi = 0.01$ and three battery pack sizes. The black solid line represents the reference power, and the black dashed lines represent SOC limits.

sizes lead to power tracking failure at the end of the simulated blackout. This enables the identification of an appropriate value of $\bar{\mu}_{tr} = 1 \times 10^{15}$. A value above this reflects that the microgrid design and controller fails to perform as required.

4.2 Optimal Microgrid Designs

To determine the relationship between the design variables and objective functions, a grid search is used to solve the CCD problem. The search uses θ from $\theta_{min} = 10000$ to $\theta_{max} = 28000$ in steps of 1000, and ϕ from $\phi_{min} = 0.01$ to $\phi_{max} = 0.06$ in steps of 0.01. While this does not guarantee the global minima is found, it provides approximate trends for the design space. Of the 114 designs, the 18 with $\theta < 13000$ violate the $\bar{\mu}_{tr}$ limit and are eliminated. Figure 6 presents the relationship between each sustainability objective function and the design variables. From this, we make the following observations:

- (a) The manufacturing objective function is only sensitive to the plant design variable, as expected from (10).
- (b) The operations objective is more sensitive to the controller, rather than the plant, design variable. Larger values of ϕ increase the total wasted energy.
- (c) The disposal objective is sensitive to both variables. Decreasing ϕ and increasing θ leads to more degradation, more component replacements, and thus more e-waste.

Comparing Figures 6(a) and 6(c) shows that J_m and J_d are generally not competing objectives in the design space. Figure 7 presents the design space comparing (a) J_m and J_o and (b) J_d and J_o , with $w_d = 0$ and $w_m = 0$ in (13), respectively. The Pareto front of Figure 7(a) indicates the manufacturing and operations sustainability objectives compete. However, as these have the same units, J_m is orders of magnitude larger than J_o . This implies that GHG emissions from manufacturing dwarf waste heat in terms of environmental impact, and

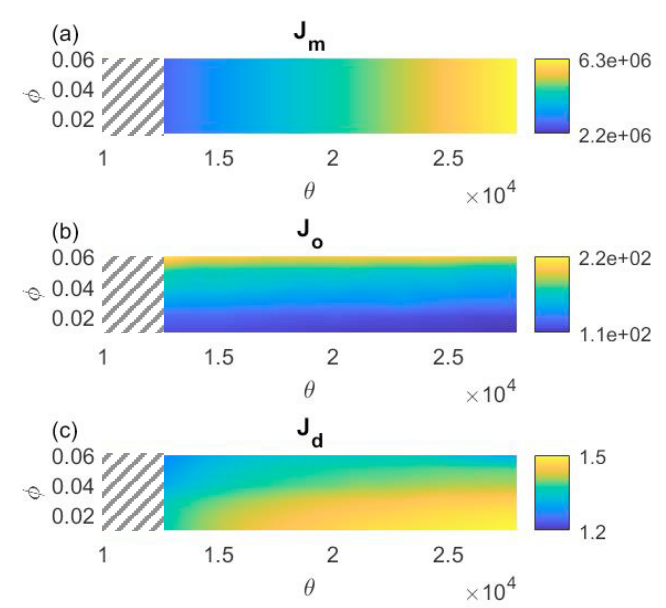


Figure 6. (a) J_m , (b) J_o , and (c) J_d versus design variable values, with gray diagonal lines indicating infeasible designs that violate $\bar{\mu}_{tr}$.

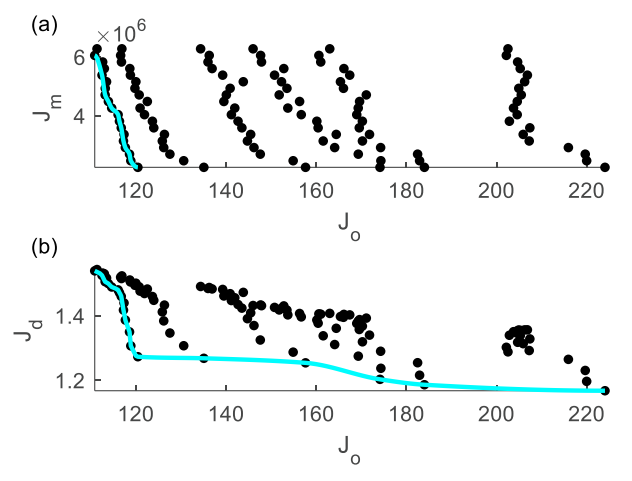


Figure 7. Design options (black) and Pareto fronts (cyan) for (a) $w_d = 0$ and (b) $w_m = 0$.

minimizing J_m minimizes J_{tot} . The magnitude of c_m , and thus J_m , would need to be reduced by 10^4 before J_o should be considered with respect to environmental impacts. For the front of Figure 7(b), the units of J_d and J_o do not match. The selection of w_o , w_d , and n in (13) determines which design to pick for a nonconvex problem such as this. There is no definitive requirement to prioritize minimizing J_d or J_o , as this will depend on the needs of the designer.

5. CONCLUSIONS

This paper presents a sustainability-centric, control co-design framework for optimal design of microgrid systems. As the requirements of energy supply and demand evolve, the environmental impact of power delivery becomes more critical. This work enables the development of next generation microgrids by optimizing both plant and controller features simultaneously with objective functions explicitly related to sustainability. The objectives are categorized based on the lifecycle stages of the microgrid components: manufacturing,

operation, and disposal. The CCD framework is tested using a candidate microgrid configuration intended to power a data center during a blackout. Results for the test scenario show that environmental impacts from manufacturing are greater than those from operations. Future work will expand on the forms and types of the sustainability objectives, and the relationship of these with multiple plant and controller design variables.

ACKNOWLEDGEMENTS

This material is based upon work supported by National Science Foundation under Award No. 2324707.

REFERENCES

- Aazami, R. et al. (2022) 'Optimal Control of an Energy-Storage System in a Microgrid for Reducing Wind-Power Fluctuations', Sustainability (Switzerland), 14(10).
- Abou El-Ela, A.A., Mosalam, H.A. and Amer, R.A. (2023) 'Optimal control design and management of complete DC- renewable energy microgrid system', *Ain Shams Engineering Journal*, 14(5).
- Ali, Z.M. *et al.* (2020) 'Variable step size perturb and observe MPPT controller by applying θ-modified krill herd algorithm-sliding mode controller under partially shaded conditions', *Journal of Cleaner Production*, 271, p. 122243.
- Alramlawi, M. and Li, P. (2020) 'Design optimization of a residential pv-battery microgrid with a detailed battery lifetime estimation model', *IEEE Transactions on Industry Applications*, 56(2), pp. 2020–2030.
- Attia, A.M. *et al.* (2021) 'A multi-objective optimization model for sizing decisions of a grid-connected photovoltaic system', *Energy*, 229.
- Barakat, S., Ibrahim, H. and Elbaset, A.A. (2020) 'Multiobjective optimization of grid-connected PV-wind hybrid system considering reliability, cost, and environmental aspects', *Sustainable Cities and Society*, 60.
- Cohen, J. et al. (2023) 'Economic Controls Co-Design of Hybrid Microgrids with Tidal/PV Generation and Lithium-Ion/Flow Battery Storage', Energies, 16(6).
- Docimo, D.J. et al. (2021) 'Plant and controller optimization for power and energy systems with model predictive control', Journal of Dynamic Systems, Measurement and Control, Transactions of the ASME, 143(8).
- Docimo, D.J. and Fathy, H.K. (2017) 'Multivariable State Feedback Control as a Foundation for Lithium-Ion Battery Pack Charge and Capacity Balancing', *Journal of The Electrochemical Society*, 164(2), pp. A61–A70.
- Docimo, D.J., Ghanaatpishe, M. and Mamun, A. (2017) 'Extended Kalman Filtering to estimate temperature and irradiation for maximum power point tracking of a photovoltaic module', *Energy*, 120, pp. 47–57.
- Fuchs, H. *et al.* (2020) 'Comparing datasets of volume servers to illuminate their energy use in data centers', *Energy Efficiency*, 13(3), pp. 379–392.
- Hao, H. *et al.* (2017) 'GHG Emissions from the production of lithium-ion batteries for electric vehicles in China', *Sustainability (Switzerland)*, 9(4).

- Jones, A.D. and Underwood, C.P. (2001) 'A thermal model for photovoltaic systems', Solar Energy, 70(4), pp. 349– 359
- Koot, M. and Wijnhoven, F. (2021) 'Usage impact on data center electricity needs: A system dynamic forecasting model', *Applied Energy*, 291.
- Laird, C. *et al.* (2022) 'Framework for integrated plant and control optimization of electro-thermal systems: An energy storage system case study', *Energy*, 258.
- Larcher, D. and Tarascon, J.M. (2015) 'Towards greener and more sustainable batteries for electrical energy storage', *Nature Chemistry*. Nature Publishing Group, pp. 19–29.
- Masaud, T.M. and El-Saadany, E.F. (2020) 'Correlating Optimal Size, Cycle Life Estimation, and Technology Selection of Batteries: A Two-Stage Approach for Microgrid Applications', *IEEE Transactions on Sustainable Energy*, 11(3), pp. 1257–1267.
- Pandit, D. et al. (2021) 'Design Optimization of Microgrid Incorporating Battery Exchange-based Electric Vehicles', in Conference Record - IAS Annual Meeting (IEEE Industry Applications Society).
- Pangborn, H.C. et al. (2018) 'Experimental validation of graph-based hierarchical control for thermal management', Journal of Dynamic Systems, Measurement and Control, Transactions of the ASME, 140(10).
- Parisio, A. and Glielmo, L. (2011) 'Energy efficient microgrid management using Model Predictive Control', in *Proceedings of the IEEE Conference on Decision and Control*. IEEE, pp. 5449–5454.
- Ramadass, P. et al. (2004) 'Development of First Principles Capacity Fade Model for Li-Ion Cells', *Journal of The Electrochemical Society*, 151(2), p. A196.
- Shehabi, A. et al. (2016) United States Data Center Energy Usage Report.
- Villalva, M.G., Gazoli, J.R. and Filho, E.R. (2009) 'Modeling and circuit-based simulation of photovoltaic arrays', in *IEEE Brazilian Power Electronics Conference*. IEEE, pp. 1244–1254.
- Wang, D. et al. (2012) 'Energy Storage in Datacenters: What, Where, and How much?', in Sigmetrics/Performance Joint International Conference on Measurement and Modeling of Computer Systems, pp. 187–198.
- Wang, H. et al. (2020) 'Optimal Control Design for Load Frequency Control with Network-induced Delays', in ICEICT 2020 - IEEE 3rd International Conference on Electronic Information and Communication Technology, pp. 664–669.
- Yan, B. et al. (2017) 'Operation and Design Optimization of Microgrids with Renewables', *IEEE Transactions on Automation Science and Engineering*, 14(2), pp. 573–585.
- Zevenhoven, R. and Beyene, A. (2011) 'The relative contribution of waste heat from power plants to global warming', *Energy*, 36(6), pp. 3754–3762.
- Zhao, T. and Ding, Z. (2018) 'Cooperative Optimal Control of Battery Energy Storage System under Wind Uncertainties in a Microgrid', *IEEE Transactions on Power Systems*, 33(2), pp. 2292–2300.